**International Conference on Applied Energy 2019**
**Aug 12-15, 2019, Västerås, Sweden**
**Paper ID: 0867**

# THERMOCHEMICAL CONVERSION OF $CO_2$ FOR THE PRODUCTION OF SYNGAS OF A SOLAR DRIVEN STEAM REFORMING IN A SOLAR PHOTO-THERMOCHEMICAL REACTOR: A THEORETICAL STUDY

Fernando Antônio de Araújo Silva Filho [1], Jornandes Dias da Silva[1]

[1]Polytechnic School - UPE, Laboratory of Environmental and Energetic Technology; Rua Benfica - 455, Madalena, Recife – PE, Brazil, Cep: 50750-470, Corresponding author: e-mail address: [*] jornandesdias@poli.br

**ABSTRACT**

High temperature heat transfer, mass transfer, and thermochemical storage performances of the solar driven $CO_2$ reforming of methane are numerically investigated along reactor length. A pseudo-homogeneous mathematical model is developed to simulate the heat and mass transfer processes coupled with thermochemical reaction kinetics in photo-thermochemical reactor with radiative heat loss. Thus, the temperature profile at the surface of the solid phase and the temperature profile in the gas phase are obtained. In addition, the conversions of reactants of $CH_4$ and $CO_2$ are studied under different operating temperatures. On the other hand, the DFR of $H_2$ and $Q_{Chem}$ are also evaluated at the operating temperature.

**Keywords:** Modelling, Reforming of $CO_2$, Solar Energy, Photo-thermochemical, Hydrogen.

## 1. INTRODUCTION

The worldwide's renewable energy is widely dominated by the burning of fossil fuels which leads to the emissions of $CO_2$ into the atmosphere and is known to contribute to the undesired global warming. The questions of fossil fuel depletion and climate change have resulted in development of solar industrial process solutions. Reforming processes which make use of solar heat to drive high temperature endothermic chemical reactions are known as solar photo-thermochemical processes. Solar photo-thermochemical reforming is based in the use of concentrated solar energy as a heating source of high temperature for conducting an endothermic chemical transformation [1]. The solar reforming technology can be used to produce renewable energies (as solar hydrogen production) as from solar photo-thermochemical reaction systems (STRSs). Actually, hydrogen ($H_2$) has a long tradition as an energy carrier and as an important raw material in chemical industries and refineries [2,3]. Theoretically, all hydrogen produced today is sourced from fossil fuels using the steam reforming of methane as principal process.

Solar driven carbon dioxide ($CO_2$) reforming of methane (SDCDRM) can be considered as a promising process for producing solar hydrogen ($H_2$). The SDCDRM is based on the utilization of concentrated solar irradiation (CSI) as an energy source to maintain high operating temperature. Accordingly, it was defined the concept of solar photo-thermochemical reactor (SPR) to study the SPR process [4]. SPR is an important and valuable device for process intensification where many applications can be carried out at high operating temperature.

In this work, a mathematical model has been developed to investigate the heat and mass transfer phenomena coupled with thermochemical reaction kinetics in SPR. The performance from SPR using the SDCDRM process is numerically investigated in terms of the temperature profiles in the gaseous and solid phases. In addition, the production of $H_2$ in SPR.

## 2. SOLAR THERMOCHEMICAL MODELLING

### *2.1 Problem description*

In the last two decades, Researches have proven the efficient use of solar thermal energy for driving highly endothermic reforming reactions. For this

Selection and peer-review under responsibility of the scientific committee of the 11th Int. Conf. on Applied Energy (ICAE2019).

purpose, a schematic setup (Figure 1) was employed to study the SRT process in STR.

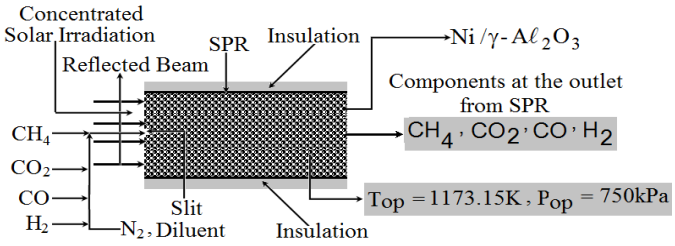


Fig 1 schematic setup from SPR

*2.2* Kinetic mechanism

In this study, the SDCDRM reaction was considered as follows.

$$CH_4 + CO_2 \rightarrow CO + 3H_2\,;\ \Delta H^0_{298K} = 206.11 kJ/mol \qquad (1)$$

The component models of these reactions are defined as toluene ($CH_4$), carbon dioxide ($CO_2$), carbon and monoxide (CO), hydrogen ($H_2$).

*2.3* Kinetic model

The global rate from Eq. (1) is defined as follows.

$$R_1 = \frac{k_1 K_{CH_4} K_{CO_2} P_{CH_4} P_{CO_2}}{\left(1 + K_{CH_4} P_{CH_4} + K_{CO_2} P_{CO_2}\right)^2}\left(1 - \frac{P_{CO}^2 P_{H_2}^2}{K_1 P_{CH_4} P_{CO_2}}\right) \qquad (2)$$

In Equation (2), $R_{CRM}$ (kmol/$kg_{cat.}$h) is the kinetic rate from CRM reaction; $k_{CRM}$ (kmol/ $kg_{cat.}$h) is the kinetic rate constant from CRM reaction, $K_{CO2}$ ($kPa^{-1}$) is the surface adsorption equilibrium constant of $CO_2$, $K_{CRM}$ ($kPa^2$) is the equilibrium constant from CRM reaction, respectively.

The net rates of each chemical components ($r_i$, i = $CH_4$, $CO_2$, CO and $H_2$) are computed in Table 1 and can be found in Reference [2].

Table 1 Net rates of components i from Eq. (1)

| Components | Equations of net rates |
|---|---|
| $CH_4$ | $r_{CH_4} = -\eta_1 R_{SDRM}$ |
| $CO_2$ | $r_{CO_2} = -\eta_1 R_{SDRM}$ |
| CO | $r_{CO} = +\eta_1 R_{SDRM}$ |
| $H_2$ | $r_{H_2} = +\eta_1 R_{SDRM}$ |

*2.4 SPR modelling approach of coupled equations*

A theoretical dynamic equation is developed to describe the heat transfer process of the gas phase on directly irradiated gas-solid SPR. Thus, the governing energy balance of the gas phase in porous medium SPR is built as follows.

- Energy balance in the gas phase;

$$\sum_{i=1}^{4} \rho_{g,i} C_{p,g,i}\left(\frac{\partial T_g}{\partial t} + \frac{4q_g}{\pi d_\mu^2}\frac{\partial T_g}{\partial z}\right) = \lambda_{g,eff}\frac{\partial^2 T_g}{\partial z^2} - h_{gs}\frac{(1-\varepsilon_b)}{\varepsilon_b}\frac{6}{d_p}\left(T_g - T_s\right);\ 0 \le z \le L_z, t > 0 \qquad (3)$$

In Equation (3), $C_{p,g}$ (kJ/kg K) is the molar heat capacity at constant pressure of the gas mixture, $T_g$ (K) is the gas temperature, z (m) is the axial direction, respectively; $\lambda_{g,eff}$ (W/m K) is the effective thermal conductivity of the gas phase, $h_{gs}$ ($W/m^2$ K) is the gas-solid heat transfer coefficient, $d_p$ (m) is the diameter of the solid particles, $T_s$ (K) is the solid temperature, respectively.

The suitable initial and boundary conditions from Eq. (3) are given as follows.

$$T_g\big|_{t=0,\ 0\le z\le L_z} = 0 \qquad (4)$$

$$\frac{\partial T_g}{\partial z}\bigg|_{z=0^+,\ t\ge 0} = \frac{\sum_{i=1}^{4}\rho_{g,i}C_{p,g,i}}{\lambda_{g,eff}}\frac{4q_g}{\pi d_\mu^2}\left(T_g\big|_{z=0^+,\ t\ge 0} - T_{g,in}\right) \qquad (5)$$

$$\frac{\partial T_g}{\partial z}\bigg|_{z=L_z,\ t\ge 0} = 0 \qquad (6)$$

The reactive packed bed consists of a particle network structure with porosity typically of about 40-60%. The thermal storage takes place on the solid particles to ensure sufficient energy for processing the endothermic reactions from the SDCDRM process. In the presence of radiation, the energy balance equation for temperature at the surface of the solid phase is given as follows.

- Energy balance at the surface of the solid phase;

$$\sum_{i=1}^{4}\rho_{s,i}C_{p,s,i}\frac{\partial T_s}{\partial t} = \left(\lambda_s\left(T_g\right) + \frac{16n^2\sigma T_\infty^3}{3k_R}\right)\frac{\partial^2 T_s}{\partial z^2} + \rho_s\frac{\left(1-\varepsilon_p\right)}{\varepsilon_p}\Delta H_1\eta_1 R_1 + h_{gs}\frac{6}{d_p}\frac{\left(1-\varepsilon_b\right)}{\varepsilon_b}\left(T_g - T_s\right) - \varepsilon_w A_{cs}\sigma\left(T_s^4 - T_\infty^4\right);\ 0 \le z \le L_z, t > 0 \qquad (7)$$

In Eq. (7), $\rho_s$ ($kg/m^3$) is the density of the solid phase, $C_{p,s}$ (kJ/kg K) is the molar heat capacity at constant pressure of the solid phase, $\lambda_s$ (W/m K) is the solid thermal conductivity, $q_{irrad.}$ ($W/m^2$) is the irradiative heat flux, $\varepsilon_p$ ($m^3$gas/$m^3$reactor) is the void fraction of the solid phase, $\Delta H_j$ (kJ/kmol) is the heat of reaction, $\eta_j$ (-) is the effectiveness factor, $R_j$ (kmol/$kg_{cat.}$

h) is the overall rate of reaction j, $\varepsilon_w$ (-) is the emissivity of wall, $A_{cs}$ ($m^2$) is the cross-cut section area, $\sigma$ ($W/m^2 T^4$) is the Stefan-Boltzmann constant, and $T_\infty$ (K) is the ambient temperature, respectively.

The suitable initial and boundary conditions from Eq. (5) are given as follows.

$$T_s\big|_{t=0,\ 0\le z\le L_z} = 0 \tag{8}$$

$$\left.\frac{\partial T_s}{\partial z}\right|_{z=0^+,t\ge 0} = \frac{DNI}{\lambda_s\left(T_{g,0}\right)} \tag{9}$$

$$\left.\frac{\partial T_s}{\partial z}\right|_{z=L_z,t\ge 0} = 0 \tag{10}$$

The mass balance equations are presented for each component i (i = $CH_4$, $CO_2$, CO and $H_2$) in SPR. A PHM model is developed to report every chemical component i in detail. In this model, it is assumed that the gas properties and flow at the inlet cross-section of the reactor are uniform. Thus, the mass balance equation of chemical components i in SPR is given as follows.

$$\varepsilon_b \frac{\partial C_i}{\partial t} + \frac{4q_g}{\pi d_\mu^2}\frac{\partial C_i}{\partial z} = \varepsilon_b D_{ax,i}\frac{\partial^2 C_i}{\partial z^2} + \rho_s \eta_1 \sum_{i=1}^{4} r_i; \tag{11}$$

$$0 \le z \le L_z, t > 0$$

In Eq. (11), $C_i$ ($mol/m^3$) is the concentration of components i at the surface of catalyst particles, $Q_g$ ($m^3$/min) is the gas flow rate, $d_\mu$ (m) is the inner diameter from SPR, $D_{ax,i}$ ($m^2$/min) is the axial mass dispersion coefficient of components i, $r_i$ ($kmol/kg_{cat.}$ min) is the net rates from components i, respectively.

The suitable initial and boundary conditions from Eq. (11) are presented as follows.

$$C_i\big|_{t=0,\ 0\le z\le L_z} = 0 \tag{12}$$

$$D_{ax,i}\left.\frac{\partial C_i}{\partial z}\right|_{z=0^+,t\ge 0} = \frac{4q_g}{\pi d_\mu^2}\left(C_i\big|_{z=0^+,t\ge 0} - C_{i,in}\right) \tag{13}$$

$$\left.\frac{\partial C_i}{\partial z}\right|_{z=L_z,t\ge 0} = 0 \tag{14}$$

## *2.5* Numerical solution of the mathematical model

The Laplace transform is used to transform the governing partial differential equations in together with their boundary conditions to a system of nonlinear ordinary equations. In present contribution, the system of the transformed equations (Eqs. (2)-(14)) in jointly with the boundary conditions are discretized by finite volume (FV) method. After the discretization from the transformed equations using the VF method, the inverse Laplace transformation is applied. It is found that the variation of integration step has negligible influence on the results obtained of this work. Therefore, an integration step of $10^{-6}$ was used to reach all the simulated results in this article.

## *2.6 Results and Discussion*

### *2.6.1. Temperature Profiles*

Figure 2 reports the temperature profile at the surface of the solid phase and the temperature profile of the gas phase along the SPR length, respectively. As shown in Figure 2, the temperature profile at the surface of the solid phase decreases from 2100K to more or less 1185K whereas the temperature profile of the gas phase increases from 300K to more or less 1185K. The temperature profiles of the solid and gas phases reach the same temperature at more or less 3.75 mm from SPR length. As from 3.75 mm, two-phase temperatures of 1185K were kept constant up to the ultimate length from SPR.

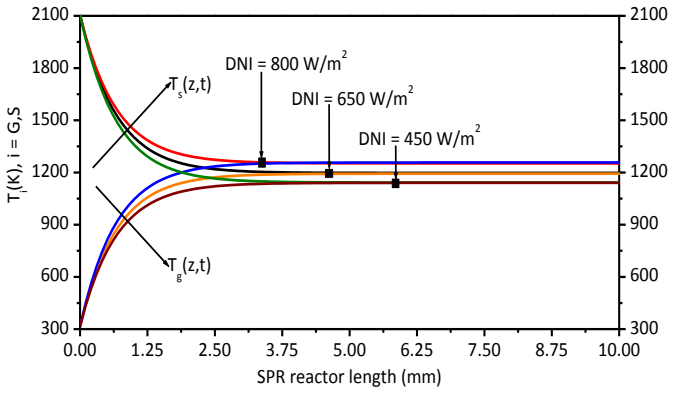


Fig 2 Temperature profile at the surface of the solid phase and the temperature profile of the gas phase.

### *2.6.2. Conversions of $CH_2$ and $CO_2$*

Figure 3 reports the effect of the operating temperature on the overall conversion of reactants ($CH_4$ and $CO_2$) on the model reaction at operating condition of 650 kPa along the packed bed from SPR with radiative heat loss. Moreover, results of the overall conversion of reactants ($CH_4$ and $CO_2$) on the model reaction were computed at five different operating temperatures. From Figure 3, the overall conversion (of $CH_4$ is achieved to be at the center of outlet surface with the values of 0.6694 (T = 925K), 0.7701 (T = 1000K), 0.8419 (T = 1075K), 0.9216 (T= 1150K), and 0.9895 (T

=1225K), respectively. On the other hand, the conversion of $CO_2$ is a little lower than the conversion of $CH_4$ at the center of outlet surface. As it was shown in Figure 3, the overall conversion of $CO_2$ is reached to be at the center of outlet surface with the values of 0.4578 (T = 925K), 0.5401 (T = 1000K), 0.5813 (T = 1075K), 0.6897 (T= 1150K), and 0.7789 (T =1225K), respectively.

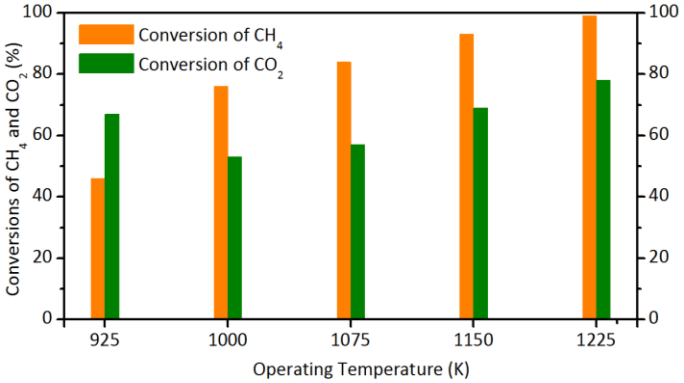


Fig 3 Conversions of $CH_4$ and $CO_2$ under different operating temperatures at the center of outlet surface from SPR.

*2.6.3. operating temperature on the DFR and $Q_{Chem}$*

A suitable method is used to compute the dimensionless flow rate (DFR) of $H_2$ relative to initial concentration of $CH_4$ of the reforming process. Effect of the operating temperature on the DFR of $H_2$ as well as the energy stored as chemical enthalpy ($Q_{Chem}$) is presented in Figure 4. As the operating temperature is raised, simulated results of the conversions of DFR of $H_2$ and $Q_{Chem}$ are remarkably increasing how it is can be seen in Figure 4. As results, the DFR of $H_2$ and $Q_{Chem}$ reach the maximum values at the operating temperature of 1225K. Thus, the DFR of $H_2$ and $Q_{Chem}$ have achieved the maximum values of 162.92 and 138.21 kJ/sec at the operating temperature of 1225K, respectively.

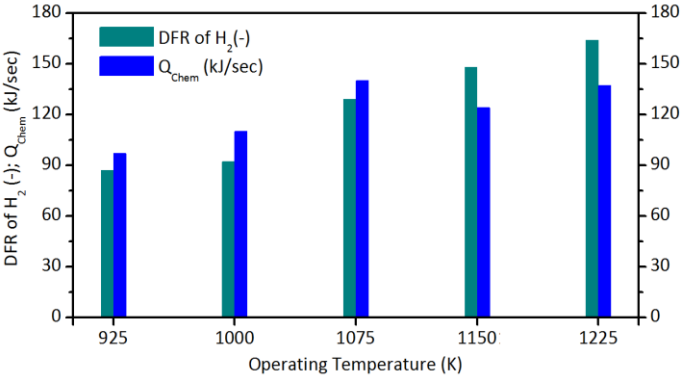


Fig 4 Effect of the operating temperature on the DFR and $Q_{Chem}$

*2.7 Conclusions*

The heat transfer and thermochemical performance of the SRT process are numerically investigated with radiative heat loss. A computer code to simulate and analyze the performance of the thermochemical process variables allowed the following conclusions:

1. The temperature profiles at the surface of the solid phase and the temperature profiles of the gas phase are sharply affected by the DNI. As results, reaction temperature at the outlet surface region has varied of $1021.26 < T_{react.} < 1245.27$K.
2. The overall conversions of reactants of $CH_4$ and $CO_2$ reached values 98.95% and 77.89%, respectively, at the operating temperature of 1225K.
3. The values of DFR of $H_2$ and $Q_{Chem}$ had reached their maximum values of 162.92 and 138.21 kJ/sec, respectively, at the operating temperature of 1225K.

**ACKNOWLEDGEMENT**

The authors of this paper would like to thank CNPq (National Council of Scientific and Technological Development) for the financial support given (Process 48354/2012).

**REFERENCE**

[1] Matienzo J M R. Influence of addition of hydrogen produced on board in the performance of a stationary diesel engine. Int J of Hydrogen Energy 2018; 43: 17889-17897. https://doi.org/10.1016/j.ijhydene.2018.07.023.

[2] Cruz B M, Silva J D. A two-dimensional mathematical model for the catalytic steam reforming of methane in both conventional fixed-bed and fixed-bed membrane reactors for the Production of hydrogen. Int J of Hydrogen Energy 2017; 42: 23670-23690. https://doi.org/10.1016/j.ijhydene.2017.03.019.

[3] Silva J D, Abreu C A M. Modelling and simulation in conventional fixed-bed and fixed-bed membrane reactors for the steam reforming of methane. Int J of Hydrogen Energy 2016; 41: 11660-11674. https://doi.org/10.1016/j.ijhydene.2016.01.083.

[4] Jin J, Wei X, Liu M, Yu Y, Li W, Kong H, Hao Y. A solar methane reforming reactor design with enhanced efficiency. Applied Energy 2018; 226: 797-807. https://doi.org/10.1016/j.apenergy.2018.04.098.